Chinese Journal of
POLYMER SCIENCE

RESEARCH ARTICLE

https://doi.org/10.1007/s10118-026-3709-3
Chinese J. Polym. Sci.

Pyrimidoisoindigo-based Polymers for Ambipolar Charge Transport

Yu-Ze Wang[a], Xiao-Yan Zhang[b], Ze-Zhou Liang[a], You-Bing Mu[a*], Zhi-Yuan Zhao[c*], Jie-Yu Wang[b], Jian Pei[b], Yun-Qi Liu[c], and Xiao-Bo Wan[a*]

[a] *Key Laboratory of Flexible Optoelectronic Materials and Technology, Ministry of Education, School of Optoelectronic Materials & Technology, Jianghan University, Wuhan 430056, China*
[b] *Beijing National Laboratory for Molecular Sciences, the Key Laboratory of Bioorganic Chemistry and Molecular Engineering of Ministry of Education, College of Chemistry and Molecular Engineering, Peking University, Beijing 100871, China*
[c] *Institute of Chemistry Chinese Academy of Sciences, Beijing 100080, China*

Electronic Supplementary Information

Abstract Two pyrimidoisoindigo-based polymers were synthesized by copolymerizing thiophene-flanked pyrimidoisoindigo (T-PymII) with thiophene (T) or 3,4-difluorothiophene (2FT), and their structure–property correlations were investigated. Although both polymers exhibited ambipolar transport properties, P(PymII-TTT) was dominated by hole transport, while P(PymII-T-2FT-T) was dominated by electron transport. Among them, the highest hole mobility up to 1.66×10^{-2} $cm^2\cdot V^{-1}\cdot s^{-1}$ was observed for P(PymII-TTT), while the highest electron mobility of 6.37×10^{-3} $cm^2\cdot V^{-1}\cdot s^{-1}$ was observed for P(PymII-T-2FT-T). AFM and GIWAXS analyses revealed that their poor morphology and crystallinity may account for their inferior performance. Therefore, further side-chain engineering is needed to improve the crystallinity of PymII-based polymers.

Keywords Pyrimidoisoindigo; Organic field-effect transistor; Ambipolar charge transport

Citation: Wang, Y. Z.; Zhang, X. Y.; Liang, Z. Z.; Mu, Y. B.; Zhao, Z. Y.; Wang, J. Y.; Pei, J.; Liu, Y. Q.; Wan, X. B. Pyrimidoisoindigo-based polymers for ambipolar charge transport. *Chinese J. Polym. Sci.* https://doi.org/10.1007/s10118-026-3709-3

INTRODUCTION

Since Tsumura *et al.*[1] made the first organic field-effect transistor (OFET) using polythiophene as the semiconductor layer in 1986, the scientific community has continued to improve its performance. According to the type of carrier transport, OFETs can be classified as p-type, n-type, or ambipolar-type. Ambipolar OFETs are an important research direction because no sophisticated micropatterns to fabricate both n- and p-channels are needed in such devices, which simplifies the large-area manufacturing of complementary integrated circuits. To date, the hole mobility of p-type polymer semiconductors has been reported to be over 50 $cm^2\cdot V^{-1}\cdot s^{-1}$,[2] whereas the electron mobility of ambipolar polymer semiconductors reaches 16.67 $cm^2\cdot V^{-1}\cdot s^{-1}$.[3] However, balancing the mobility of both electrons and holes in ambipolar conjugated polymers remains difficult. Similar to n-type semiconductors, ambipolar polymers require low lowest unoccupied molecular orbital (LUMO) energy levels for stable electron-transport behaviours,[4] which calls for the design of acceptors with higher electron deficiencies.[5,6] On the other hand, they also need to have suitable highest occupied molecular orbital (HOMO) energy levels that allow efficient hole transport, which means that relatively small bandgaps compared to those of n-type and p-type conjugated polymers are required.[7] In addition to these factors, different aggregation behaviours and crystallinities of the conjugated polymers also have a significant influence on the final outcome of device performance. However, there is no clear guidance for designing a donor-acceptor (D-A)-type conjugated polymer fulfilling all three criteria; therefore, trial-and-error methods are still needed to find a suitable acceptor for better ambipolar charge transport behaviors. A general method is to manipulate the existing acceptors for lower LUMO energy levels and then test how such a structural change will lead to changes in the properties of the polymer in the solid state and the mobility of the devices.

Isoindigo has a long history of use as a building block for the synthesis of conjugated polymers for OFETs.[8] In 2010, Reynolds' team[9] introduced isoindigo as an acceptor unit into conjugated oligomers for the first time, and used the obtained organic semiconductor materials for organic photovoltaics. Isoindigo has two lactams in its molecular structure, endowing it with a LUMO energy level of approximately −3.60 eV,[10] so it has been widely used as the acceptor to construct D-A-type polymers since then. In 2011, Pei *et al.*[11] synthesized IIDT and IIDDT by copolymerizing isoindigo with bis(trimethylstannyl)thiophene or 5,5′-bis(trimethyl-stannyl)-2,2′-bithiophene, which are the first series of isoindigo-based copolymers. Among them, IIDDT exhibits a hole mobility of up to 0.79 $cm^2\cdot V^{-1}\cdot s^{-1}$. The hole mobility can be further increased to 3.62 $cm^2\cdot V^{-1}\cdot s^{-1}$ by adjusting the branching point

* Corresponding authors, E-mail: muyb@jhun.edu.cn (Y.B.M.)
E-mail: zhaozhiyuan@iccas.ac.cn (Z.Y.Z.)
E-mail: wanxb@jhun.edu.cn (X.B.W.)
Received December 29, 2025; Accepted April 14, 2026; Published online July 20, 2026

of the alkyl side chains away from the polymer backbones.[12] They also synthesized a series of isoindigo-based copolymers with different donors, all of which exhibited p-type transport behaviour because the LUMO energy level was not low enough[13]. Among them, the copolymer with terthiophene (P(IID-TTT)) (Fig. 1a, left structure) has the most linear backbone and exhibits a hole mobility of up to 0.061 $cm^2 \cdot V^{-1} \cdot s^{-1}$. Subsequently, they introduced electron-withdrawing substituents such as F and Cl onto the isoindigo core, which lowered the LUMO energy level of the acceptors, and the corresponding polymers exhibited ambipolar transport behaviour.[14,15]

On the other hand, electron-deficient heterocycles have also been used to replace the phenyl ring in the isoindigo core in order to lower the LUMO level of polymers. In 2016, García-Frutos *et al.*[16] replaced the benzene ring in isoindigo with an electron-deficient pyridine ring and synthesized 7,7′-diazaisoindigo (7DAII), whose LUMO energy level decreased to −3.84 eV.[17] Almost at the same time, Yu's team[18] further simplified the synthesis route toward dibromo-7DAII (7DAII-Br_2) and copolymerized it with 5,5′-bis(trimethyl stannyl)-2,2′-bithiophene or 2,5-bis(trimethylstannyl)-thieno[3,2-*b*]thiophene, resulting in diazaisoindigo-based polymers[18,19] that exhibited ambipolar transport behaviour with hole/electron mobility of 2.33/0.78 and 1.14/1.54 $cm^2 \cdot V^{-1} \cdot s^{-1}$, respectively. Pei *et al.*,[17] on the other hand, reported the synthesis of dibromo-5,5′-diazaisoindigo (5DAII-Br_2), which had an even lower LUMO energy level (−3.92 eV) than 7DAII-Br_2. However, its copolymer with 5,5′-bis(trimethyl stannyl)-2,2′-bithiophene exhibited p-type charge transport behaviour, probably because of its nearly amorphous morphology without observable crystalline domains.[17] Yue *et al.*[20,21] synthesized P(7DAII-TTT) (Fig. 1a, middle structure), which is a hole-transporting semiconductor material with a mobility up to 0.62 $cm^2 \cdot V^{-1} \cdot s^{-1}$. It appears that increasing the conjugated length of the donor units makes the DAII-based polymer less preferable for ambipolar transport. In 2018, our group[10] reported the synthesis of thiazoloisoindigo (TzII) by replacing the benzene ring in isoindigo with an electron-deficient thiazole ring; its LUMO energy level was reduced to −3.68 eV. The copolymer of TzII with terthiophene (P(TzII-TTT))[22] (Fig. 1a, right structure) is an ambipolar transport material dominated by hole transport, with hole mobility of 3.93 $cm^2 \cdot V^{-1} \cdot s^{-1}$ and electron mobility of 1.07 $cm^2 \cdot V^{-1} \cdot s^{-1}$. TzII can form a quinoidal structure more easily than DAII, which allows better delocalization of the LUMO along the polymer chain, accounting for its ambipolar behavior compared with p-type P(7DAII-TTT), which has the same donor units. We[23–26] also synthesized a series of TzII-based copolymers, which all exhibited ambipolar transport behavior, and among them, the copolymer of thiophene-flanked TzII and thiophene-flanked diketopyrrolopyrrole P(T-TzII-T-DPP) exhibited balanced and high hole and electron mobility (5.77 $cm^2 \cdot V^{-1} \cdot s^{-1}$ for hole and 6.29 $cm^2 \cdot V^{-1} \cdot s^{-1}$ for electron, respectively).

Recently, our group reported the successful synthesis of thiophene-flanked pyrimidoisoindigo (T-PymII) [27] by replacing the benzene ring in isoindigo with an even more electron-deficient pyrimidine ring. The LUMO energy level of T-PymII was lowered to −3.91 eV, and a wider LUMO/HOMO energy gap (2.06 eV) was observed, showing that T-PymII is a strong electron-acceptor that may be suitable to construct n-type or

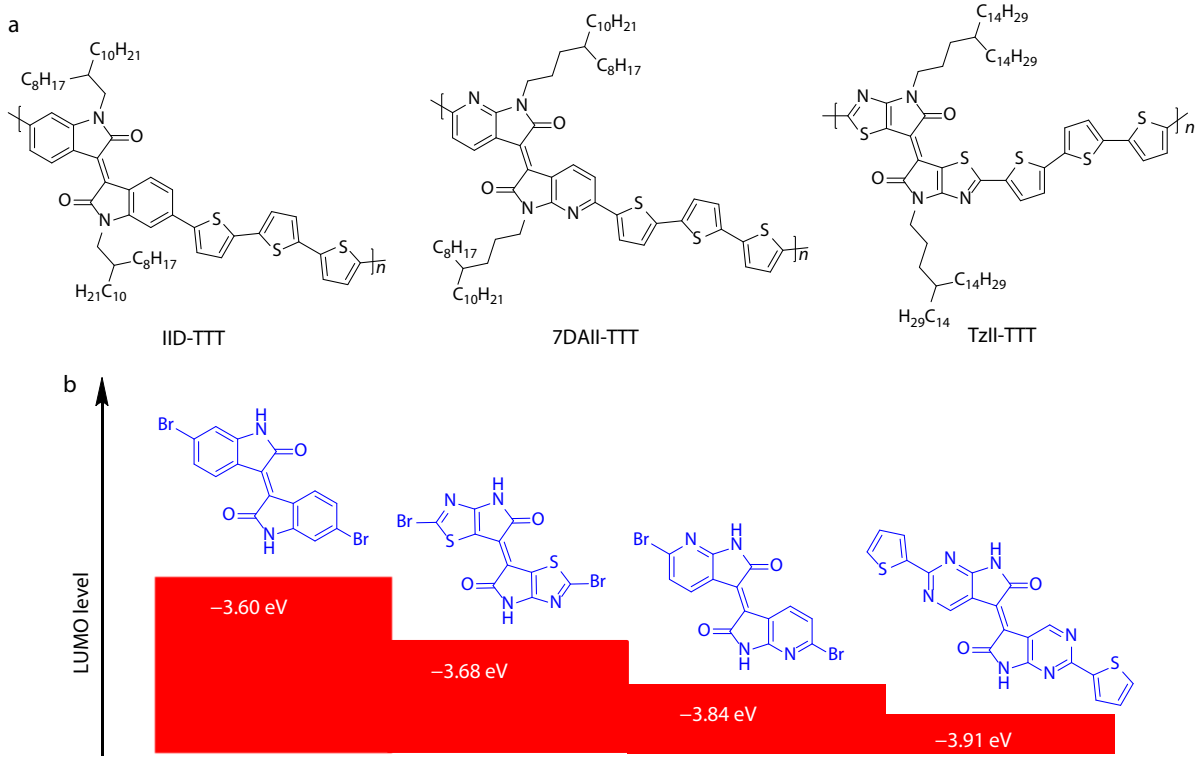

Fig. 1 Reported modifications on the isoindigo core: (a) molecular structures of IID-Br_2, TzII-Br_2, DNIID-Br_2 and T-PymII and their relative LUMO energy levels; (b) representative structures of polymers based on IID, AIID and TzII with terthiophene.

https://doi.org/10.1007/s10118-026-3709-3

ambipolar conjugated polymers. Fig. 1(b) shows the LUMO energy level of T-PymII compared to that of other isoindigo-derived acceptors. Herein, we prepared two new polymers based on T-PymII, namely P(PymII-TTT) and P(PymII-T-2FT-T), by easy copolymerization with bis(trimethylstannyl)-thiophene and 2,5-bis(trimethylstannyl)-3,4-difluorothiophene, respectively, and tested their OFET performances. The results showed that both polymers exhibited ambipolar transport behaviour, and a preference for electron transport was observed for P(PymII-T-2FT-T). However, the mobility of both polymers is not high because of their poor crystallinity, although theoretical calculations have shown that both have a planar backbone. Further modifications may be needed to optimize the performance of PymII-based polymers.

EXPERIMENTAL

All the experimental procedures and details are available in the article and electronic supplementary information (ESI).

RESULTS AND DISCUSSION

Monomer Synthesis and Polymerization

The synthetic routes to T-PymII-Br are shown in Scheme 1. The synthesis of 2-chloro-7*H*-pyrrolo-[2,3-*d*]pyrimidine (compound **1**) has been reported in our previous work.[27] To guarantee the solubility of the resultant polymers, compound **1** was alkylated with a C24-chain with the branch point four-carbon away from the nitrogen atom in 90% yield. The reactive C-2 position of the pyrimidine ring was protected by attaching a thiophene ring *via* Stille coupling, resulting in compound **3** in 70% yield. Treating compound **3** with NBS in *t*-butanol containing 5% H_2O afforded 3,3-dibromo-5,7-azaoxindole (**4**) in 75% yield without affecting the thiophene ring. Dibromide **4** was reacted with $AgNO_3$ to obtain thiophene-flanked 5,7-azaisatin (compound **5**) in 82% yield. By reducing dibromide **4** with zinc powder under acidic conditions, 5,7-azaindolin-2-one **6** was obtained in 85% yield. T-PymII was then synthesized through an aldol condensation reaction between compounds **5** and **6** in 60% yield. Finally, monomer T-PymII-Br (compound **8**) was obtained by bromination with NBS in 70% yield. Detailed characterization data of the compounds are provided in ESI.

The syntheses of the two T-PymII-based polymers are shown in Scheme 2. The polymerization of T-PymII-Br with bis-stannylated thiophene or 3,4-difluoro-thiophene *via* Pd-catalyzed Stille cross-coupling afforded P(PymII-TTT) and P(PymII-T-2FT-T), respectively. Both polymers were precipitated in methanol and then sequentially extracted by Soxhlet extraction using hexane, ethyl acetate, and dichloromethane to remove oligomers and other impurities, and the final products were dissolved in chloroform under reflux conditions and precipitated in methanol to give dark-red solids in 90% yield and 93% yield, respectively. The M_ns values of the two polymers were characterized by high-temperature gel permeation chromatography using trichlorobenzene as the eluent at 150 °C (Fig. S1 in ESI), and the results are summarized in Table 1. Polymers with similar molecular weights (49.7 kDa versus 48.1 kDa) and similar polydispersity indices (*Đ*) (2.33 versus 2.16) were obtained. DSC measurements (Fig. S2 in ESI) indicated that no phase transition or thermal degradation was observed in the microstructure of either polymer from room temperature to 300 °C. Both polymers exhibited high thermal stability with decomposition temperatures of approximately 413 and 397 °C, respectively (Fig. S3 in ESI).

Density Functional Theory Calculation

We selected the Density Functional Theory (DFT) method at the B3LYP-D3(BJ)/def2TZVP computational level for geometry optimization characterization, using PymII-TTT and PymII-T-2FT-T dimers as model compounds. The HOMO/LUMO energy-level distributions are shown in Fig. 2(a). In both cases, the LUMO and HOMO are well distributed along the dimer backbones, showing that the introduction of a fluorine atom in the donor unit does not significantly change the distribution of the HOMO/LUMO. The calculated HOMO/LUMO energy levels of the PymII-T-2FT-T dimer are −5.57/−3.61 eV, which are deeper than those of PymII-TTT (−5.44/−3.55 eV), which is consistent with the experimental results. The planarity of both the polymers was calculated based on the dimers, and the results are shown in Fig. 2(b). Both polymers were quite planar, with only a small dihe-

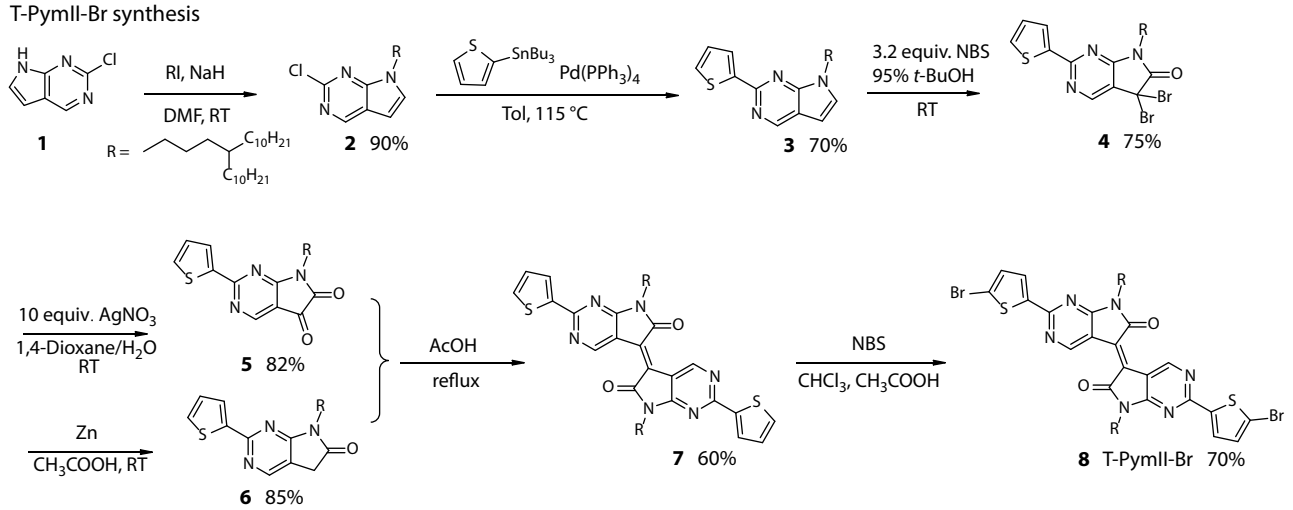

Scheme 1 Synthetic routes to the T-PymII-Br.

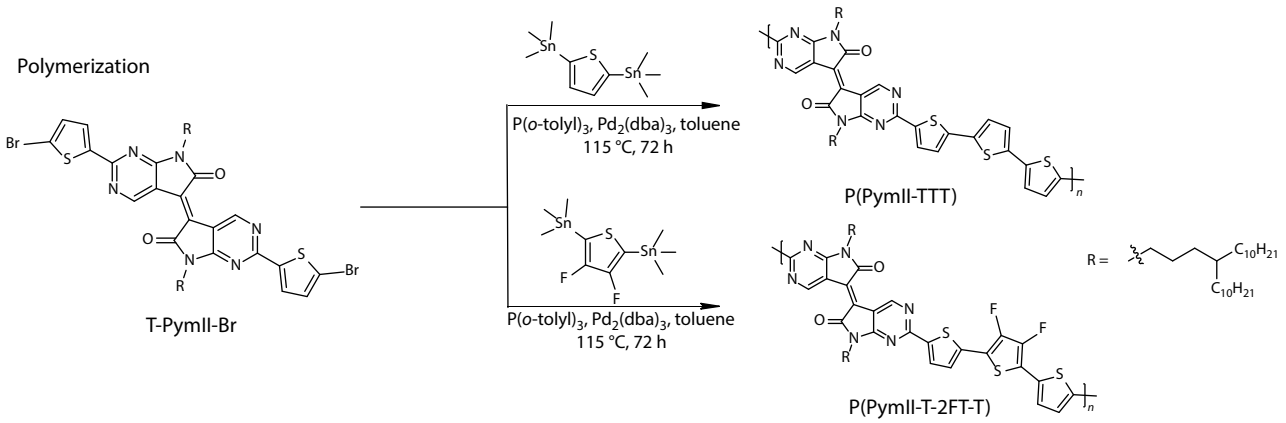

Scheme 2 Synthetic routes to P(PymII-TTT) and P(PymII-T-2FT-T).

Table 1 Photophysical properties and electronic properties of PymII-TTT and PymII-T-2FT-T.

Sample	M_n [a] (kDa)	PDI [a]	λ_{max} (nm)/λ_{onset} (nm)		$E_{g,opt}$ [d] (eV)	Exp. [e] (CV)		$E_{g,CV}$ [f] (eV)
			Solution [b]	Film [c]		HOMO (eV)	LUMO (eV)	
P(PymII-TTT)	49.7	2.33	425, 663, 698/784	425, 647, 705/789	1.57	−5.70	−3.83	1.87
P(PymII-T-2FT-T)	48.1	2.16	403, 636, 680/745	402, 636, 693/757	1.64	−5.81	−3.98	1.83

[a] Measured in 1,2,4-trichlorobenzene at 150 °C by size exclusion chromatography; [b] Absorption maxima and onset of absorption in chloroform solution (1×10^{-5} g/mL); [c] Absorption maxima and onset of absorption in thin film; [d] Optical bandgaps were confirmed by absorption onset of the thin film with $E_{g,opt} = 1240/\lambda$; [e] HOMO and LUMO were calculated from the oxidation and reduction potentials, respectively; [f] $E_{g,CV} = E_{LUMO} - E_{HOMO}$.

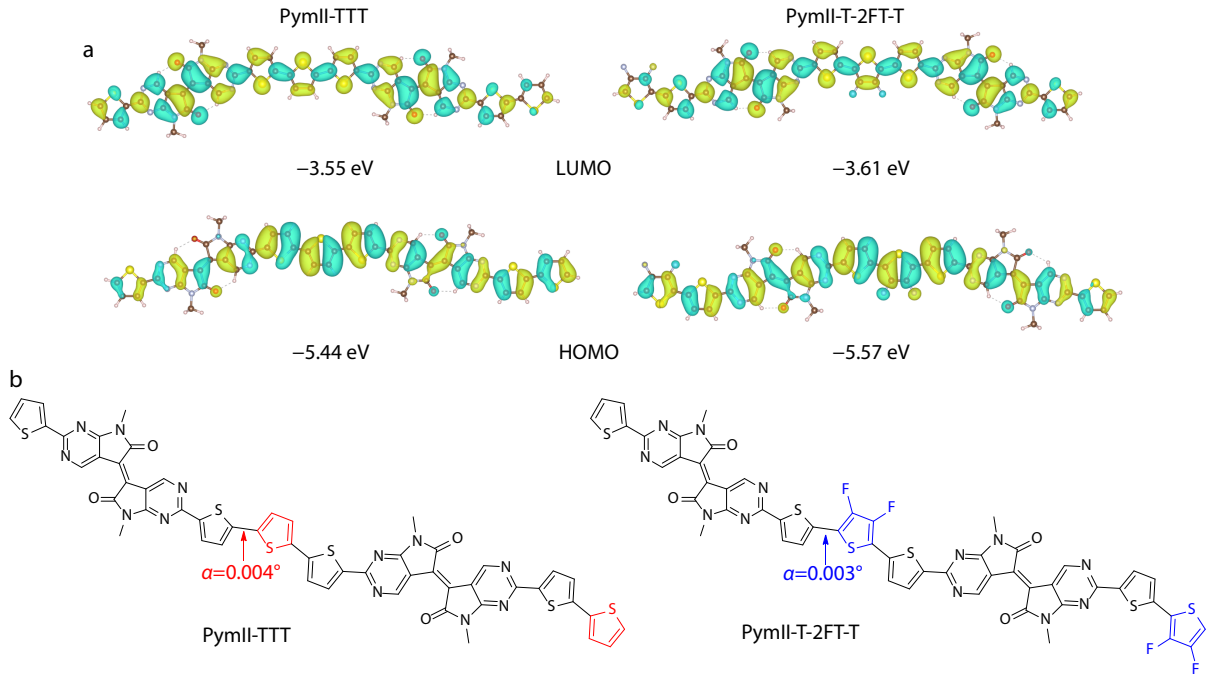

Fig. 2 (a) The calculated HOMO/LUMO energy level distribution for the PymII-TTT and PymII-T-2FT-T dimers; (b) Calculated dihedral angles of PymII-TTT and PymII-T-2FT-T dimers.

dral angle difference between the thiophene rings in PymII-TTT (α=0.004°) and the thiophene and 3,4-difluorothiophene rings in PymII-T-2FT-T (α=0.003°), probably because of the formation of F···S secondary orbital interactions.

Electrochemical and Optical Properties

Cyclic voltammetry (CV) tests were used to characterize the electrochemical bandgaps ($E_{g,eV}$) of the two T-PymII-based polymers, and the redox potentials are summarized in Table 1, with the corresponding cyclic voltammetry (CV) diagrams presented in the Supporting Information (Fig. S4 in ESI). The HOMO/LUMO levels identified by CV are −5.70/−3.83 eV for P(PymII-TTT) and −5.81/−3.98 eV for P(PymII-T-2FT-T), respectively. P(PymII-T-2FT-T) showed nearly 0.15 eV lower LUMO level and 0.11 eV lower HOMO level than that of P(PymII-TTT), showing that the introduction of a fluorine atom on the thiophene ring had a signifi-

cant effect on its energy levels. The $E_{g,eV}$ of P(PymII-TTT) and P(PymII-T-2FT-T) are 1.87 and 1.83 eV, respectively.

The UV-Vis-near-infrared (UV-Vis-NIR) absorption spectra of both polymers were measured in chloroform and in thin film state, as shown in Fig. 3 and the data are summarized in Table 1. In the solution state, P(PymII-TTT) exhibits a red-shifted maximum absorption peak with an absorption onset at 784 nm compared with P(PymII-T-2FT-T), which is attributed to its narrower optical bandgap. The optical bandgap ($E_{g,opt}$) was found to be 1.57 eV for P(PymII-TTT), which is obviously smaller than that (1.64 eV) of P(PymII-T-2FT-T), indicating that the introduction of a fluorine atom on the thiophene ring leads to a wider bandgap. P(PymII-T-2FT-T) exhibits distinguishable 0-0 and 0-1 absorption peaks, illustrating that P(PymII-T-2FT-T) may have a more rigid planar skeleton conformation than P(PymII-TTT), presumably because of the F···S interaction, which makes the conformation more rigid. Compared with those in the solution state, the absorption spectra of the two polymers in the thin-film state exhibited only a slight red shift. It can be seen from Fig. 3 that in the thin film state, both polymer exhibit clear 0-0 and 0-1 vibrational peaks compared to the solution state, which indicates that the rigidity of the polymers in the aggregated state is improved.

Charge Transport Properties in OFET Devices

The carrier transport properties of the polymers were studied by fabricating OFETs with top-gate/bottom-contact (TG/BC) and bottom-gate/bottom-contact (BG/BC) configurations. Detailed OFET parameters are provided in Tables S1 and S2 (in ESI). The transfer and output characteristic curves of the OFETs are shown in Figs. 4 and 5, and the relevant performance parameters are listed in Table 2. The devices constructed using the two polymers exhibit ambipolar transport properties, in which P(PymII-TTT) is dominated by hole transport, while P(PymII-T-2FT-T) is dominated by electron transport, probably because P(PymII-T-2FT-T) has a lower LUMO level. In TG/BC devices, P(PymII-TTT) shows an average hole mobility of 1.1×10^{-2} $cm^2\cdot V^{-1}\cdot s^{-1}$, while its electron mobility is 3 times lower (3.5×10^{-3} $cm^2\cdot V^{-1}\cdot s^{-1}$). P(PymII-T-2FT-T) shows an average hole mobility of 3.8×10^{-4} $cm^2\cdot V^{-1}\cdot s^{-1}$, while its electron mobility is 12 times higher (4.6×10^{-3} $cm^2\cdot V^{-1}\cdot s^{-1}$). In BG/BC devices, P(PymII-TTT) shows an average hole mobility of 1.3×10^{-3} $cm^2\cdot V^{-1}\cdot s^{-1}$, while its electron mobility is 30 times lower (4.0×10^{-5} $cm^2\cdot V^{-1}\cdot s^{-1}$). P(PymII-T-2FT-T) shows an average hole mobility of 2.1×10^{-5} $cm^2\cdot V^{-1}\cdot s^{-1}$, while its electron mobility is 15 times higher (3.2×10^{-4} $cm^2\cdot V^{-1}\cdot s^{-1}$). A clear preference for electron transport by P(PymII-T-2FT-T) was observed in both device configurations. The V_{th} values for both polymers are relatively high owing to the high density of surface defects and charge traps that immobilize charge carriers and suppress efficient charge accumulation at the dielectric-semiconductor interface.

Morphology and Aggregation State Characterization

The relatively inferior OFET performance of both PymII-based polymers compared to DAII-based polymers or TzII-based polymers prompted us to investigate the reasons that led to such

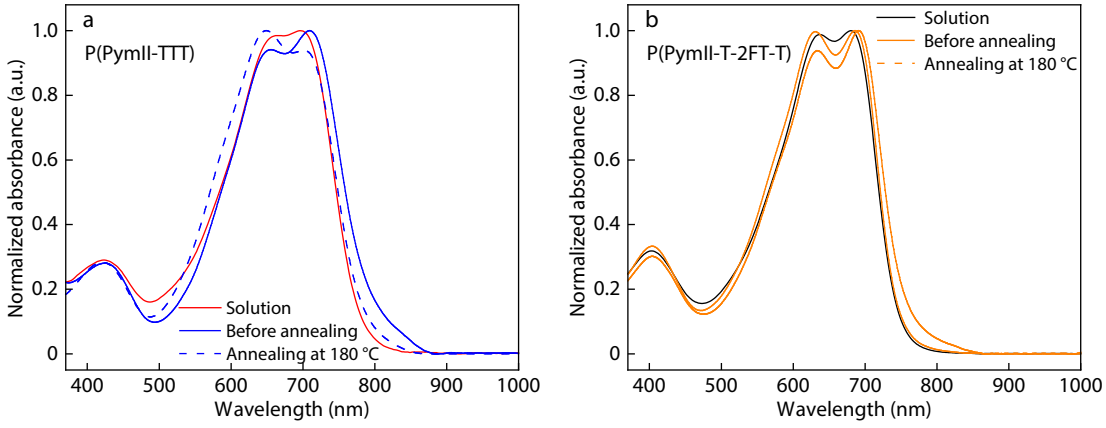

Fig. 3 UV-Vis-NIR absorption spectra of the polymers (a) P(PymII-TTT) and (b) P(PymII-T-2FT-T) in chloroform solution (1×10^{-5} g/mL) and thin films.

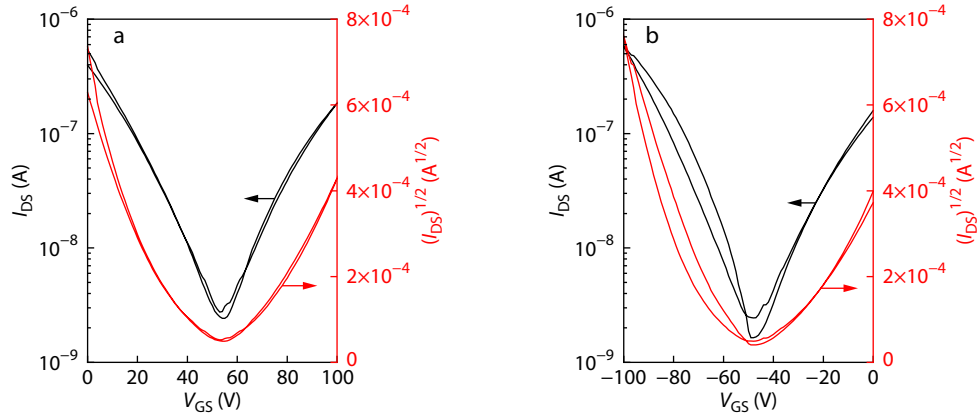

https://doi.org/10.1007/s10118-026-3709-3

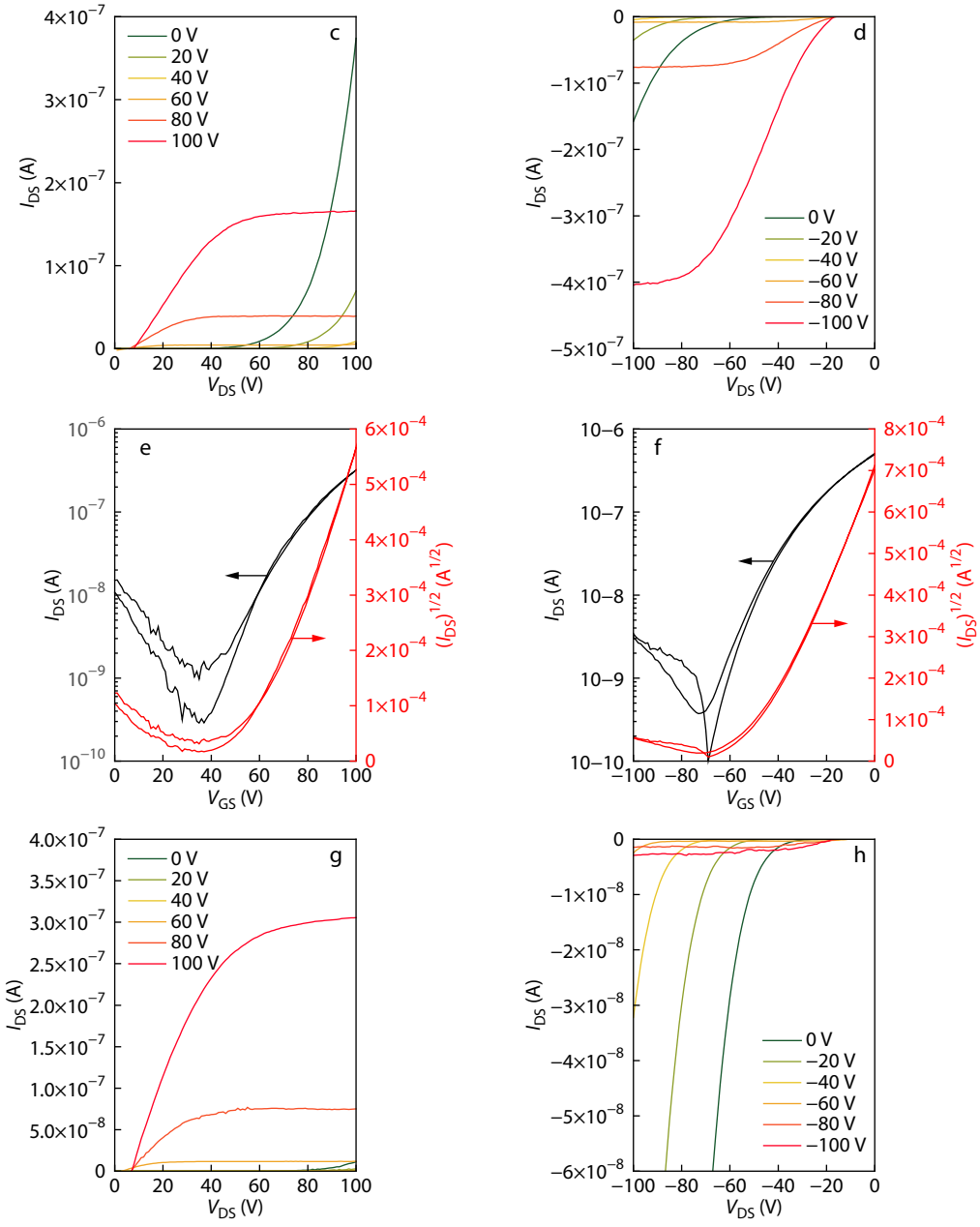

Fig. 4 Transfer and output characteristics of (a–d) P(PymII-TTT); (e–h) P(PymII-T-2FT-T) in TG-BC devices.

unexpected results, since PymII is an even better acceptor when judged by its lower LUMO energy level. Therefore, the morphologies and crystallinities of both the polymers were investigated. The film quality and surface morphology were characterized by AFM in the tapping mode. Both polymers show root-mean-square roughness (RMS) values of 1.03 and 1.32 nm, respectively, as seen in Fig. 6. Notably, no clear nanofibers can be observed for either P(PymII-TTT) or P(PymII-T-2FT-T) films, which may account for the poor performance of the devices. However, there are also examples showing that a smooth surface may lead to high mobility; therefore, this may not be the only reason. The crystallinity of both polymers was investigated, and Fig. 7 shows the 2D-GIWAXS images of both polymers before and after annealing. The GIWAXS patterns of both polymers exhibited only one distinct (100) diffraction peak in the q_{xy} direction, and no higher (h00) diffraction peaks were observed. No (100) diffraction peak can be observed in the q_z direction, showing that both polymers adopted a majorly face-on orientation, which is not a preferred orientation for charge transport. After annealing, the (100) diffraction peak was slightly enhanced; however, no higher-order (h00) peaks appeared, indicating that annealing only marginally improved the crystallinity of the polymer. The in-plane and out-of-plane GIWAXS plots of the two polymers are shown in Figs. S5 and S6 (in ESI), and the corresponding data are summarized in Table 3. The low crystallinity of both polymers may account for their mobility. Further side-chaining engineering may be required to improve the crystallinity of PymII-based polymers. There are many examples

https://doi.org/10.1007/s10118-026-3709-3

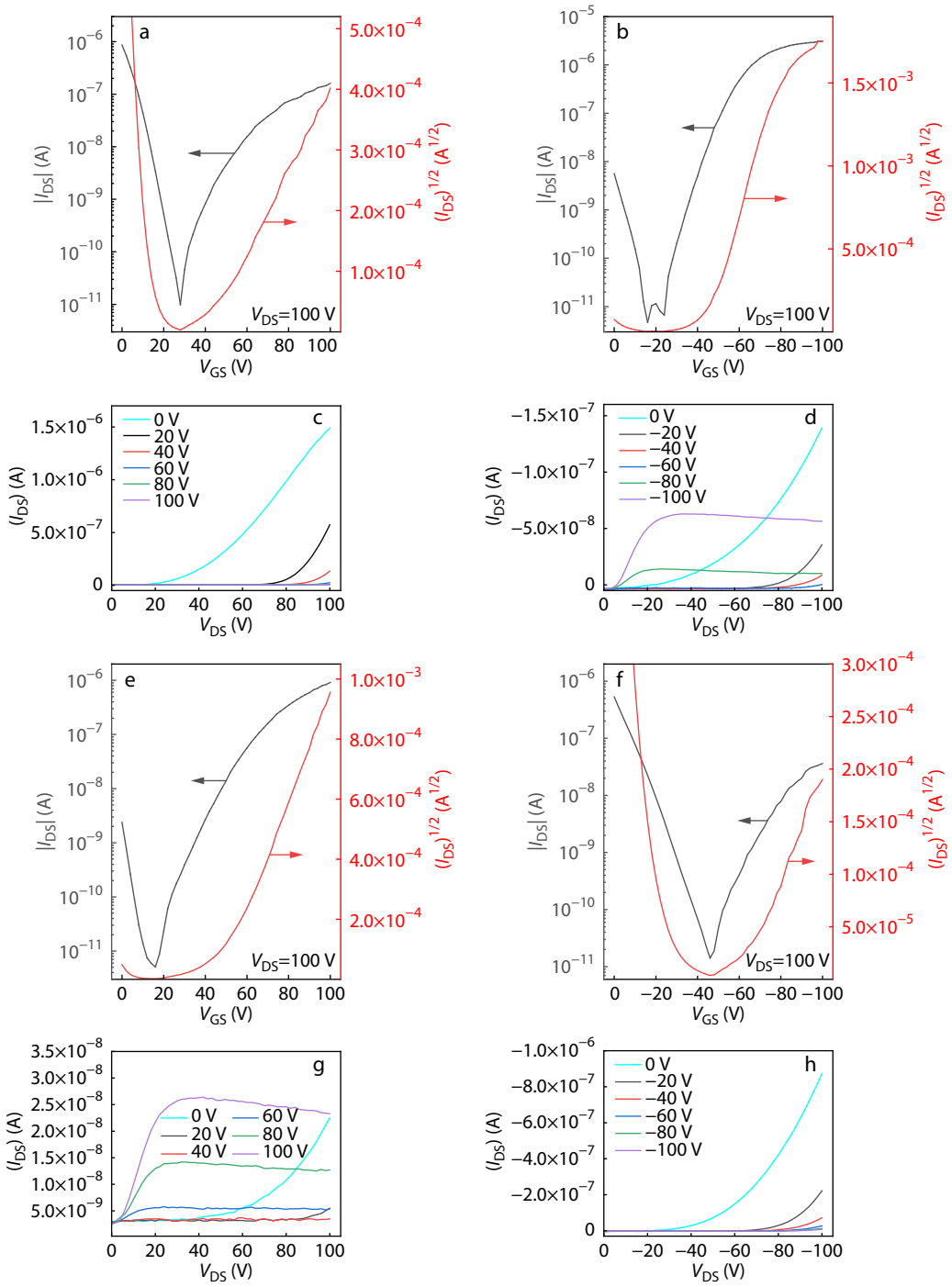

Fig. 5 Transfer and output characteristics of (a–d) P(PymII-TTT); (e–h) P(PymII-T-2FT-T) in BG-BC devices.

Table 2 OFET device performances for P(PymII-TTT) and P(PymII-T-2FT-T).

Polymer	Device architecture	$\mu_{h,max}$ ($\mu_{h,ave}$) ($cm^2 \cdot V^{-1} \cdot s^{-1}$)	$V_{th,h}$ (V)	I_{on}/I_{off}	$\mu_{e,max}$($\mu_{e,ave}$) ($cm^2 \cdot V^{-1} \cdot s^{-1}$)	$V_{th,e}$ (V)	I_{on}/I_{off}
P(PymII-TTT)	TG-BC	$1.7(1.1)\times10^{-2}$	−45	10^2–10^3	$5.2(3.5)\times10^{-3}$	60	10^3–10^4
	BG-BC	$1.5(1.3)\times10^{-3}$	−20	10^5–10^6	$4.5(4.0)\times10^{-5}$	30	10^4–10^5
P(PymII-T-2FT-T)	TG-BC	$1.1(0.4)\times10^{-3}$	−60	10^3–10^4	$6.4(4.6)\times10^{-3}$	40	10^3–10^4
	BG-BC	$2.5(2.1)\times10^{-5}$	−50	10^5–10^6	$3.6(3.2)\times10^{-4}$	20	10^5–10^6

showing that optimizing side chains may lead to higher crystallinity, such as using silylcarbon or siloxyl side-chains to replace hydrocarbon side-chains, which is quite promising, as summarized in several recent reviews.[28,29]

https://doi.org/10.1007/s10118-026-3709-3

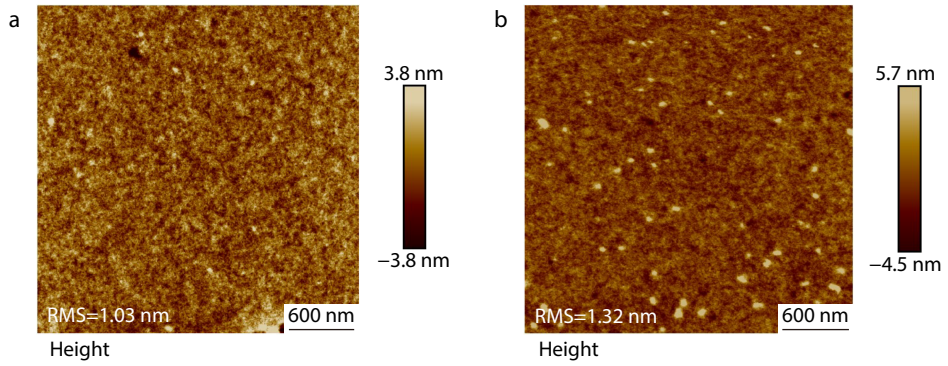

Fig. 6 AFM images of the polymers (a) P(PymII-TTT) and (b) P(PymII-T-2FT-T).

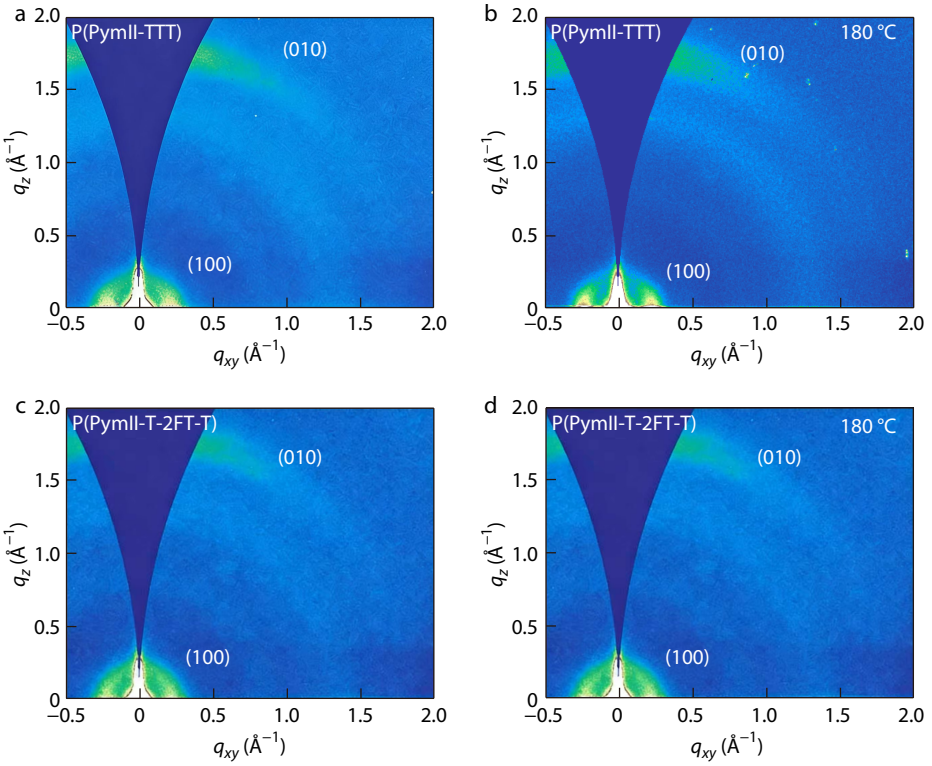

Fig. 7 2D GIWAXS patterns of (a, b) P(PymII-TTT) and (c, d) P(PymII-T-2FT-T) before (a, c) and after (b,d) annealing.

Table 3 Peak positions and d-spacings of the polymer films of P(PymII-TTT) and P(PymII-T-2FT-T) fabricated under the optimal conditions for OFET devices.

Polymer	Out-of-plane π-π (Å^{-1})	$d_{\pi\text{-}\pi}$ (Å)	In-plane lamellar (Å^{-1})	d_L (Å)
P(PymII-TTT)	1.68	3.7	0.22	28.6
P(PymII-T-2FT-T)	1.64	3.8	0.23	27.3

CONCLUSIONS

In conclusion, we designed and synthesized two T-PymII-based polymers, P(PymII-TTT) and P(PymII-T-2FT-T), by copolymerizing them with bis(trimethylstannyl)-thiophene and 2,5′-bis(trimethyl stannyl)-3,4-difluorothiophene, respectively. Both polymers have deep HOMO/LUMO energy levels (−5.70/−3.83 eV for P(PymII-TTT)) and −5.81/−3.98 eV for P(PymII-T-2FT-T), respectively). OFET devices based on P(PymII-TTT) and P(PymII-T-2FT-T) exhibited ambipolar transport behavior, and P(PymII-T-2FT-T) showed a better tendency toward electron transport. However, the charge carrier mobilities of both polymers were not high, probably because of the low crystallinity and inferior morphology in the film state. These results indicate that side-chain engineering is needed to further improve the crystallinity of PymII-based polymers for better OFET performance, which is currently underway in our laboratory.

Conflict of Interests

The authors declare no interest conflict.

https://doi.org/10.1007/s10118-026-3709-3

Electronic Supplementary Information

Electronic supplementary information (ESI) is available free of charge in the online version of this article at http://doi.org/10.1007/s10118-026-3709-3.

Data Availability Statement

The data related to this work are available on reguest.

ACKNOWLEDGMENTS

This work was financially supported by the National Natural Science Foundation of China (Nos. 22371093 and 22373048) and Hubei Provincial Natural Science Foundation of China (No. 2023 AFB1030).

REFERENCES

1 Tsumura, A.; Koezuka, H.; Ando, T. Macromolecular electronic device: Field-effect transistor with a polythiophene thin film. *Appl. Phys. Lett.* **1986**, *49*, 1210–1212.
2 Yao, Y.; Dong, H.; Liu, F.; Russell, T. P.; Hu, W. Approaching intra- and interchain charge transport of conjugated polymers facilely by topochemical polymerized single crystals. *Adv. Mater.* **2017**, *29*, 1701251.
3 Zhang, W.; Shi, K.; Lai, J.; Zhou, Y.; Wei, X.; Che, Q.; Wei, J.; Wang, L.; Yu, G. Record-high electron mobility exceeding 16 $cm^2 V^{-1} s^{-1}$ in bisisoindigo-based polymer semiconductor with a fully locked conjugated backbone. *Adv. Mater.* **2023**, *35*, 2300145.
4 Chen, X.; Feng, L.; Yu, P.; Liu, C.; Lan, J.; Lin, Y.; Yang, X. Flexible thermoelectric films based on Bi_2Te_3 nanosheets and carbon nanotube network with high n-type performance. *ACS Appl. Mater. Interfaces* **2021**, *13*, 5451–5459.
5 Qu, D.; Qi, T.; Huang, H. Acceptor–acceptor-type conjugated polymer semiconductors. *J. Energy Chem.* **2021**, *59*, 364–387.
6 Sun, H.; Guo, X.; Facchetti, A. High-performance n-type polymer semiconductors: applications, recent development, and challenges. *Chem* **2020**, *6*, 1310–1326.
7 Zhao, Y.; Guo, Y.; Liu, Y. 25th Anniversary article: recent advances in n-type and ambipolar organic field-effect transistors. *Adv. Mater.* **2013**, *25*, 5372–5391.
8 Zhu, M.; Guo, Y.; Liu, Y. A thriving decade: rational design, green synthesis, and cutting-edge applications of isoindigo-based conjugated polymers in organic field-effect transistors. *Sci. China Chem.* **2022**, *65*, 1225–1264.
9 Mei, J; Graham, K.; Stalder, R.; Reynolds, J. Synthesis of isoindigo-

Graphical Abstract

Pyrimidoisoindigo-based Polymers for Ambipolar Charge Transport

Yu-Ze Wang, Xiao-Yan Zhang, Ze-Zhou Liang, You-Bing Mu, Zhi-Yuan Zhao, Jie-Yu Wang, Jian Pei, Yun-Qi Liu, and Xiao-Bo Wan

Jianghan University; Peking University; Institute of Chemistry Chinese Academy of Sciences

Two new polymers based on thiophene-flanked pyrimidoisoindigo (T-PymII) were synthesized by copolymerizing it with thiophene and 3,4-difluorothiophene; both polymers exhibited ambipolar transport properties: P(PymII-TTT) was dominated by hole transport, while P(PymII-T-2FT-T) was dominated by electron transport.

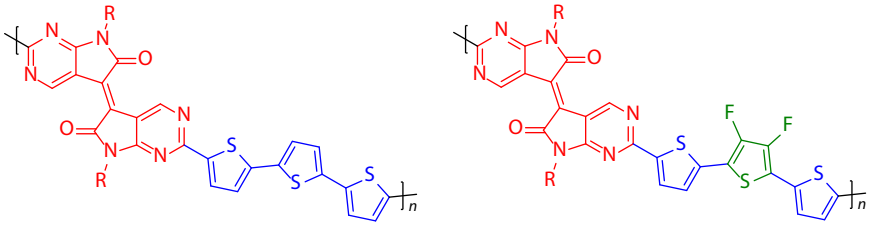

P(PymII-TTT)
μ_h=1.1×10^{-2} cm^2·V^{-1}·s^{-1}
μ_e=3.5×10^{-3} cm^2·V^{-1}·s^{-1}
μ_e/μ_h= 0.32

P(PymII-T-2FT-T)
μ_h= 3.8×10^{-4} cm^2·V^{-1}·s^{-1}
μ_e= 4.6×10^{-3} cm^2·V^{-1}·s^{-1}
μ_e/μ_h=12.11

Hole-dominated | Electron-dominated

Ambipolar transport

Chinese J. Polym. Sci., 2026 *https://doi.org/10.1007/s10118-026-3709-3*

based oligothiophenes for molecular bulk heterojunction solar cells. *Org. Lett.* **2010**, *12*, 660–663.
10 Li, C.; Zhang, H.; Mirie, S.; Peng, J.; Cai, M.; Wang, X.; Lan, Z.; Wan, X. A new approach to thiazoloisoindigo and derivatives using a lithium tetramethylpiperidine promoted cyclization to thiazoloisatin. *Org. Chem. Front.* **2018**, *5*, 442–446.
11 Lei, T.; Cao, Y.; Fan, Y.; Liu, C.; Yuan, S.; Pei, J. High-performance air-stable organic field-effect transistors: isoindigo-based conjugated polymers. *J. Am. Chem. Soc.* **2011**, *133*, 6099–6101.
12 Lei, T.; Dou, J.; Pei, J. Influence of alkyl chain branching positions on the hole mobilities of polymer thin-film transistors. *Adv. Mater.* **2012**, *24*, 6457–6461.
13 Lei, T.; Cao, Y.; Zhou, X.; Peng, Y.; Bian, J.; Pei, J. Systematic investigation of isoindigo-based polymeric field-effect transistors: design strategy and impact of polymer symmetry and backbone curvature. *Chem. Mater.* **2012**, *24*, 1762–1770.
14 Lei, T.; Dou, J.; Ma, Z.; Yao, C.; Liu, C.; Wang, J.; Pei, J. Ambipolar polymer field-effect transistors based on fluorinated isoindigo: high performance and improved ambient stability. *J. Am. Chem. Soc.* **2012**, *134*, 20025–20028.
15 Lei, T.; Dou, J.; Ma, Z.; Liu, C.; Wang, J.; Pei, J. Chlorination as a useful method to modulate conjugated polymers: balanced and ambient-stable ambipolar high-performance field-effect transistors and inverters based on chlorinated isoindigo polymers. *Chem. Sci.* **2013**, *4*, 2447–2452.
16 de Miguel, G.; Camacho, L.; García-Frutos, E. 7,7′-Diazaisoindigo: a novel building block for organic electronics. *J. Mater. Chem. C* **2016**, *4*, 1208–1214.
17 Lu, Y.; Liu, Y.; Dai, Y.; Yang, C.; Un, H.; Liu, S.; Shi, K.; Wang, J.; Pei, J. 5,5′-Diazaisoindigo: an electron-deficient building block for donor–acceptor conjugated polymers. *Chem. Asian J.* **2017**, *12*, 302–307.
18 Huang, J.; Mao, Z.; Chen, Z.; Gao, D.; Wei, C.; Zhang, W.; Yu, G. Diazaisoindigo-based polymers with high-performance charge-transport properties: from computational screening to experimental characterization. *Chem. Mater.* **2016**, *28*, 2209–2218.
19 Huang, J.; Chen, Z.; Mao, Z.; Gao, D.; Wei, C.; Lin, Z.; Li, H.; Wang, L.; Zhang, W.; Yu, G. Tuning frontier orbital energetics of azaisoindigo-based polymeric semiconductors to enhance the charge-transport properties. *Adv. Electron. Mater.* **2017**, *3*, 1700078.
20 Yue, W.; Li, C.; Tian, X.; Li, W.; Neophytou, M.; Chen, H.; Du, W.; Jellett, C.; Chen, H.; Onwubiko, A.; McCulloch, I. Diazaisoindigo bithiophene and terthiophene copolymers for application in field-effect transistors and solar cells. *J. Polym. Sci. A Polym. Chem.* **2017**, *55*, 2691–2699.
21 Yue, W.; Nikolka, M.; Xiao, M.; Sadhanala, A.; Nielsen, C.; White, A.; Chen, H.; Onwubiko, A.; Sirringhaus, H.; McCulloch, I. Azaisoindigo conjugated polymers for high performance n-type and ambipolar thin film transistor applications. *J. Mater. Chem. C* **2016**, *4*, 9704–9710.
22 Li, C.; Un, H.; Peng, J.; Cai, M.; Wang, X.; Wang, J.; Lan, Z.; Pei, J.; Wan, X. Thiazoloisoindigo: a building block that merges the merits of thienoisoindigo and diazaisoindigo for conjugated polymers. *Chem. Eur. J.* **2018**, *24*, 9807–9811.
23 Li, B.; Zou, X.; Xiong, M.; Li, Q.; Kang, X.; Mu, Y.; Wang, J.; Pei, J.; Yang, C.; Lan, Z.; Wan, X. Thiazoloisoindigo-based ambipolar polymers for excellent balanced hole and electron mobility. *Mater. Chem. Front.* **2022**, *6*, 3369–3381.
24 Lv, S.; Li, Q.; Li, B.; Wang, J.; Mu, Y.; Li, L.; Pei, J.; Wan, X. Thiazole-flanked thiazoloisoindigo as a monomer for balanced ambipolar polymeric field-effect transistors. *Chinese J. Polym. Sci.* **2022**, *40*, 1131–1140.
25 Li, B.; Xiong, M.; Liu, M.; Li, Z.; Sang, L.; Xiong, Z.; Xiao, B.; Pei, J.; Wan, X. Thiazoloisoindigo-based polymer semiconductors: synthesis, structure-property relationship, charge carrier polarity, and field-effect transistor performance. *Chinese J. Polym. Sci.* **2023**, *42*, 24–31.
26 Li, B.; Zou, X.; Li, Q.; Sang, H.; Mu, Y.; Wang, J.; Pei, J.; Yang, C.; Li, L.; Wan, X. Alternating copolymers of thiophene-flanked thiazoloisoindigo and thiophene-flanked benzothiadiazole for high-performance ambipolar organic field-effect transistors. *Org. Electron.* **2023**, *113*, 106708.
27 Wei, T.; Sun, Q.; Yang, W.; Zhang, J.; Chen, X.; Mu, Y.; Lan, Z.; Liu, C.; Wan, X. Tetrazaisoindigos: serpentine syntheses and their expected and unexpected photophysical and electronic properties. *Chem. Eur. J.* **2024**, *30*, e202402199.
28 Luo, N.; Ren, P.; Feng, Y.; Shao, X.; Zhang, H.; Liu, Z. Side-chain engineering of conjugated polymers for high-performance organic field-effect transistors. *J. Phys. Chem. Lett.* **2022**, *13*, 1131–1146.
29 Lv, S.; Li, L.; Mu, Y.; Wan, X. Side-chain engineering as a powerful tool to tune the properties of polymeric field-effect transistors. *Polym. Rev.* **2021**, *61*, 520–552.

https://doi.org/10.1007/s10118-026-3709-3